Journal of the European Ceramic Society **11** (1993) 533–543

Phase Evolution during Sintering of Bi–Ti-Doped Zinc Oxide

A. Peigney, H. Andrianjatovo, R. Legros, A. Rousset

Laboratoire de Chimie des Matériaux Inorganiques, URA CNRS No. 1311, Université Paul Sabatier, 118 Route de Narbonne, 31062 Toulouse Cedex, France

&

J. J. Couderc

Laboratoire de Physique des solides, URA CNRS No. 74, UPS et INSA, Complexe Scientifique de Rangueil, 31077 Toulouse Cedex, France

(Received 14 February 1992; revised version received 24 June 1992; accepted 1 July 1992)

Abstract

Phase evolution and localization during sintering of spherical Bi–Ti-doped zinc oxide powders were studied by X-ray diffraction and transmission electron microscopy. Several minor phases were identified on quenched ceramics; a phase, either amorphous or crystalline, stable at a wide range of compositions, originating from solidification of the melt phase during quenching, was detected. Sintering processes were discussed: depending on the Ti content, densification, liquid-phase occurrence and grain growth are quite different.

Die Lokalisierung und die Entwicklung der Phasenbildung beim Sintern sphärischer Bi–Ti-dotierter Zinkoxid-Pulver wurden mittels Röntgenbeugung und Transmissionselektronenmikroskopie untersucht. Im abgeschreckten Zustand konnten mehrere sekundäre Phasen in den Keramiken identifiziert werden. Es konnte die Existenz einer Phase ermittelt werden, die in einem weiten Zusammensetzungsbereich und entweder in amorpher oder in kristalliner Struktur vorliegt. Diese Phase entsteht durch die Erstarrung der flüssigen Phase beim Abschrecken. Die einzelnen Vorgänge beim Sintern wurden diskutiert. Entsprechend dem Ti-Gehalt sind das Verdichtungsverhalten, der Anteil flüssiger Phase und das Kornwachstum sehr verschieden.

L'évolution et la localisation des phases lors du frittage de poudres sphériques d'oxyde de zinc dopées au Bi et au Ti ont été étudiées par diffraction des rayons X et par microscopie électronique à transmission. Plusieurs phases minoritaires ont été identifiées sur les céramiques trempées; une phase, rencontrée à l'état amorphe et à l'état cristallisé, stable dans un large domaine de composition et provenant de la solidification de la phase liquide lors de la trempe a été détectée. Les processus de frittage ont été discutés: selon la teneur en titane, la densification, l'apparition de la phase liquide et le grossissement des grains sont très différents.

1 Introduction

Zinc oxide ceramics with small amounts of other metal oxides exhibit non-ohmic characteristics.[1] For low voltage applications, very large grains are required; such ceramics are made by liquid-phase sintering. Bismuth oxide is generally added as melting phase.

Trontelj *et al.*[2] have reported that in the microstructure of TiO_2-containing materials, large grains (100–200 μm) are observed in a matrix of much smaller grains. They have also shown that the average grain size increases up to 1 mol% of TiO_2 and decreases with larger additions; they inferred that Ti ions rapidly distribute in the molten Bi_2O_3 phase and increase the chemical reaction of Bi_2O_3 toward ZnO particles, thereby accelerating the coarsening of the microstructure; they identified several minor phases such as Zn_2TiO_4 spinel, $Bi_4Ti_3O_{12}$ and Bi_2O_3 in these systems.[3] No solubility of TiO_2 in ZnO could be detected in ceramics obtained by

Journal of the European Ceramic Society 0955-2219/93/$6.00

sintering of $ZnO–Bi_2O_3–TiO_2$ or $ZnO–Bi_{12}TiO_{20}$ mixtures.[4] Studies on formation reactions of ceramics prepared by mixing powders of ZnO and $Bi_4Ti_3O_{12}$ led Makovec & Trontelj[5] to propose a reaction between these two compounds which occurs above 1040°C, resulting in a spinel phase Zn_2TiO_4 and a Bi_2O_3-rich melt; the addition of $Bi_4Ti_3O_{12}$ enhances grain growth, as in the case when TiO_2 and Bi_2O_3 are separately added to the composition. Kiseleva *et al.*[6] detected $Zn_2Ti_3O_8$, Zn_2TiO_4 and $Bi_4Ti_3O_{12}$ and have not detected any reaction between ZnO and $Bi_4Ti_3O_{12}$ but only melting of $Bi_4Ti_3O_{12}$ approaching 1200°C; they inferred a two-step liquid sintering: below 1200°C, due to Bi_2O_3, which is retained by gradual reaction with TiO_2, and above 1200°C, by melting of $Bi_4Ti_3O_{12}$. For Sung & Kim,[7] the effect of 0·5 mol% TiO_2 added to the system $ZnO–Bi_2O_3–MnO$ on the enhancement of grain growth in ceramics sintered between 900 and 1200°C appeared only in the sample sintered at 1200°C. Note that all these previously mentioned studies were conducted on ceramics prepared by the usual technology (oxide mixtures).

Doped zinc oxide powders with controlled morphology obtained by the aqueous coprecipitation method have been prepared in this laboratory.[8] Liquid-phase sintering studies of bismuth–titanium-doped zinc oxide powders with spherical morphology have been conducted by dilatometry.[9] In systems 1% Bi, y% Ti (% metal atoms), shrinkage begins at a lower temperature with $y = 0{\cdot}6$ (825°C) than with $y = 1$ (950°C), the faster shrink (rearrangement stage) being revealed by the derived curve of relative shrinkage with respect to temperature occurring respectively at 845°C and 1030°C. The first composition leads to much larger grains (mean size 100 μm) than the second (mean size 55 μm). In this work, the authors have studied phase evolution and localization during the densification stage of sintering, i.e. between 750°C and 1100°C. In this way the sintering processes of these ceramics have been analysed in order to explain in particular why the optimal content of titanium necessary to obtain the larger grains in the present systems is 0·6%. Moreover, the sintering processes of bismuth–titanium-doped zinc oxide powders prepared by coprecipitation[8,9] are compared with those of oxide mixtures.[3–7]

2 Experimental Techniques

2.1 Sample preparation

Powders of doped zinc oxide, prepared by coprecipitation and calcination, were made of spherical grains of mean diameter 5 μm. Each sphere is constituted of primary particles of a size ranging from 50 to 100 nm.[8,9] The amounts of dope (atomic percentage of the total amount of metal atoms) were confirmed by plasma emission spectroscopy. Powders were mixed with an organic binder and pressed into disk form (6 mm in diameter, 1·5 mm thick) by applying a uniaxial pressure of 200 MPa.

Two series of specimens were prepared with the following atomic percentages of metals atoms:

Series A:	98·4% Zn	0·6% Ti	1% Bi
Series B:	98·0% Zn	1% Ti	1% Bi

Thermal treatments were performed in atmospheric air using a tubular furnace. Specimens were heated at a rate of 7°C/min to the desired temperature (between 750°C and 1100°C) and then quenched immediately in salted ice-cold water.

2.2 Characterization

X-Ray diffraction experiments were performed on a powder automatic diffractometer Siemens with filtered Co K_α radiation ($\lambda = 0{\cdot}17\,902$ nm) collimated by Solers slit.

For transmission electron microscopy (TEM) observation and microanalysis, the specimens were cut with a wire-saw into 100-μm slices, then mechanically ground down to 50 μm and finally thinned by ion-milling. They were observed with a JEOL 200 CX electron microscope operated at 200 kV (TEM-SCAN service of the University Paul Sabatier, Toulouse, France). Thin film X-ray spectroscopy was performed on the same electron microscope fitted with an energy-dispersive lithium-drifted silicon detector, a standard STEM attachment and an EDAX spectrum analyser unit. Semi-quantitative analysis with an accuracy of about 2–3% is available by this technique. The minimum electron probe diameter was about 10–20 nm. The oxygen content could not be measured.

Observations by scanning electron microscopy (SEM) of etched polished ceramics surfaces were conducted to reveal grain sizes with greater accuracy than by TEM.

3 Experimental Results

3.1 X-Ray diffraction results

A portion of the X-ray diffraction diagrams are shown in Fig. 1(a) (series A) and in Fig. 1(b) (series B). They were performed on ceramics quenched from 750°C, 850°C, 1000°C and 1100°C for samples belonging to series A, and from 750°C, 900°C, 1030°C and 1100°C for those from series B. Moreover, in both cases, diagrams of oxide powder, prepared by calcination of a precursor at 600°C, were also recorded. Note that 850°C and 1030°C are, for

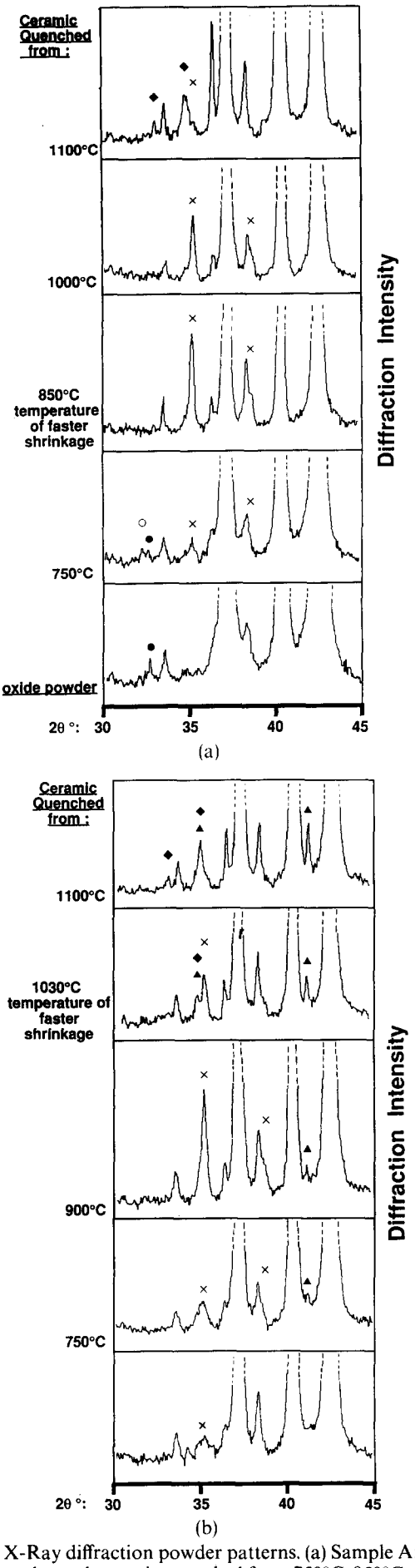

Fig. 1. X-Ray diffraction powder patterns. (a) Sample A: initial oxide powder and ceramic quenched from 750°C, 850°C, 1000°C and 1100°C; (b) sample B: oxide powder and ceramic quenched from 750°C, 900°C, 1030°C and 1100°C. (●) β-Bi_2O_3, (○) γ-Bi_2O_3, (×) $Bi_4Ti_3O_{12}$, (▲) α-Zn_2TiO_4, (◆) unidentified phase.

samples of series A and B, the temperatures of faster shrinkage as revealed by the previous dilatometric study.[9]

It is first worth noting that an X-ray diffraction pattern for a pure ZnO powder was conducted with the same apparatus conditions: in addition to the normal lines of the hexagonal structure, extra lines appeared. They fit to the diffraction of the Co K_β radiation ($\lambda = 0{\cdot}16\,207$ nm) by the hexagonal lattice. Effectively, in spite of the utilization of an appropriate filter (Fe filter in this work), residual K_β radiation can appear.[10] These extra lines must be taken into account, especially the three lines at $2\theta = 33{\cdot}5°$, $2\theta = 36{\cdot}3°$ and $2\theta = 38{\cdot}2°$ in the diagrams (Fig. 1(a) and (b)).

3.1.1 Series A samples

It is shown that four phases are generally detected (Fig. 1(a)):

(i) ZnO (with the above-mentioned extra lines).

(ii) β-Bi_2O_3. This bismuth oxide, which has a quadratic structure ($a = 1{\cdot}095$ nm, $c = 0{\cdot}563$ nm[11]), only appears up to 750°C in a very small proportion. Note that, at the same quenching temperature, γ-Bi_2O_3 (cubic centred $a = 1{\cdot}0\,245$ nm,[12] $d_{310} = 0{\cdot}324$ nm) could be present.

(iii) $Bi_4Ti_3O_{12}$. This phase has an orthorhombic structure ($a = 0{\cdot}5449$ nm, $b = 3{\cdot}2815$ nm, $c = 0{\cdot}5410$ nm[13]), the most intense line being (117) for $2\theta = 35{\cdot}07°$. It is readily apparent that the $Bi_4Ti_3O_{12}$ content is at a maximum at temperatures close to 850–1000°C.

(iv) An unidentified phase, poorly crystallized. It appears particularly at the higher quenching temperatures. The main interplanar distances corresponding to these phases are $d_1 = 0{\cdot}3155 \pm 0{\cdot}0006$ nm and $d_2 = 0{\cdot}2997 \pm 0{\cdot}0006$ nm, the latter being the most intense.

3.1.2 Series B samples

Four phases are generally present (Fig. 1(b)): ZnO, $Bi_4Ti_3O_{12}$, α-Zn_2TiO_4 and an unidentified phase. No bismuth oxide is observed, even for the powder or at low quenching temperatures. The orthorhombic $Bi_4Ti_3O_{12}$ is not detected for 1100°C-quenched samples and the maximal content of this compound is for 900°C quenching. However, a new phase is identified: α-Zn_2TiO_4, with cubic spinel structure $a = 0{\cdot}84\,602$ nm;[14] the most intense lines (311) ($d_1 = 0{\cdot}2552$ nm), (220) ($d_2 = 0{\cdot}2995$ nm) and (440) ($d_3 = 0{\cdot}1495$ nm) are clearly visible, particularly at high temperature. This phase seems to be present as soon as 750°C is reached and its content increases with quenching temperature. The unidentified phase, present only at 1100°C as before, is the same

as in series A, since the interplanar distances are similar: $d_1 = 0{\cdot}3155 \pm 0{\cdot}0006$ nm, $d_2 = 0{\cdot}2996 \pm 0{\cdot}0006$ nm, d_2 being superposed onto the α-Zn_2TiO_4 (220) line; this phase could also be present in smaller quantity at 1030°C ($d_2 = 0{\cdot}3001 \pm 0{\cdot}0006$ nm) but the absence of the d_1 line does not allow that to be asserted.

3.2 TEM observations

TEM observations have been achieved after quenching at two or three selected characteristic temperatures on each series of samples.

3.2.1 Series A samples

3.2.1.1 Quenched from 900°C. Three phases are identified by electron diffraction:

(i) ZnO with grain size ranging from 0·2 to 2 μm. Each grain was extremely rich in lattice defects such as nearly straight or loop dislocations (Fig. 2) which probably result from quenching. ZnO was also observed as amorphous or nanocrystallized zones giving broad electron diffraction rings.

(ii) $Bi_4Ti_3O_{12}$ (Fig. 3) was present as plate-like inclusions 0·5–1 μm in length and 0·1–0·3 μm in width. This compound is clearly identified by the electron diffraction patterns (Fig. 4). It is located on ZnO grain boundaries (cf. Figs 2 and 3) with the (001) plane parallel to the plate axis. High-resolution electron microscopy (HREM) allows the imaging of the lattice fringes belonging to the (002) planes ($d = 1{\cdot}64$ nm). As can be seen in Fig. 5, some stacking faults in the (001) planes are present in these compounds. The EDX microanalysis leads to an atomic ratio Bi/Ti = $1{\cdot}30 \pm 0{\cdot}03$ which fits perfectly with the $Bi_4Ti_3O_{12}$ formula but the presence of Zn atoms in the lattice cannot be excluded.

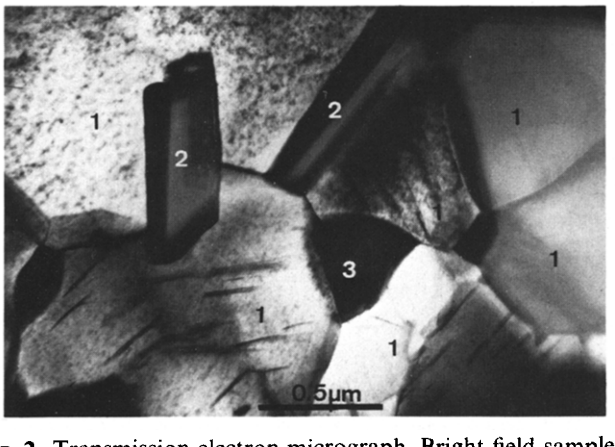

Fig. 2. Transmission electron micrograph. Bright field sample A quenched from 900°C. ZnO grains (1) with lattice defects, rods of $Bi_4Ti_3O_{12}$ (2) and γ-Bi_2O_3 grains (3) at multiple grain junctions.

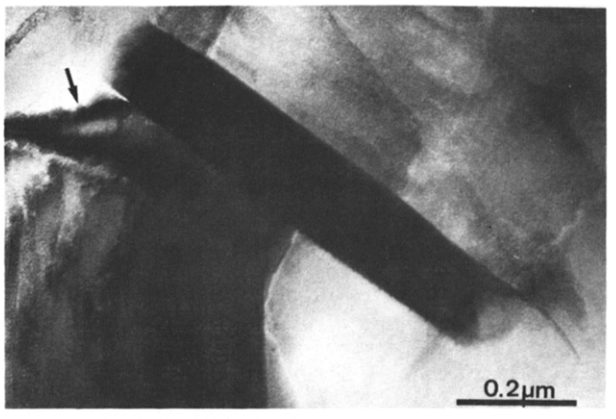

Fig. 3. Transmission electron micrograph. Bright field sample A quenched from 900°C. Rod of $Bi_4Ti_3O_{12}$ and an unidentified intergranular phase (→).

(iii) Occasional grains of γ-Bi_2O_3 (cubic centred $a = 1{\cdot}0245$ nm[12]). Selected area electron diffraction pattern areas agree with this structure (Fig. 6), which forms from the β-phase by cooling from 800°C according to the literature.[12] This phase was present on ZnO multiple grain junctions (Fig. 2). Moreover, note on Fig. 3 the occasional presence of an intergranular non-identified phase.

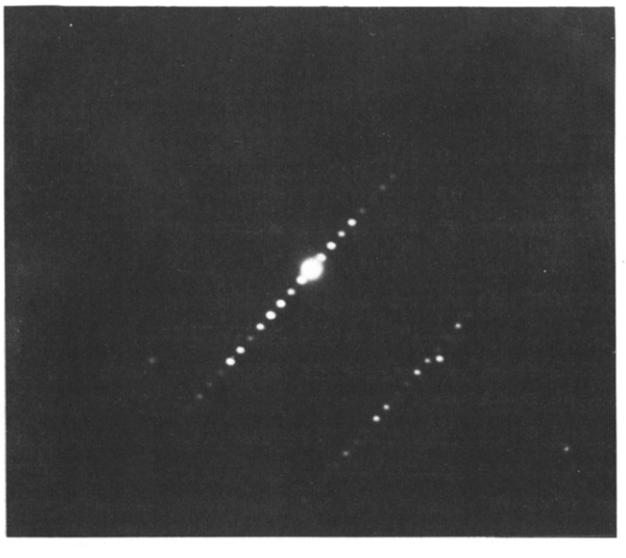

(a)

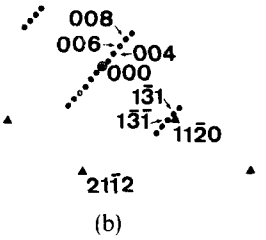

(b)

Fig. 4. (a) Transmission electron diffraction pattern of a $Bi_4Ti_3O_{12}$ rod. (b) Interpretation. (●) Reflections of $Bi_4Ti_3O_{12}$ oriented with [$\bar{3}$10) parallel to the electron beam. The (002) forbidden spot is excited by multiple reflection. (▲) Reflections of the ZnO matrix.

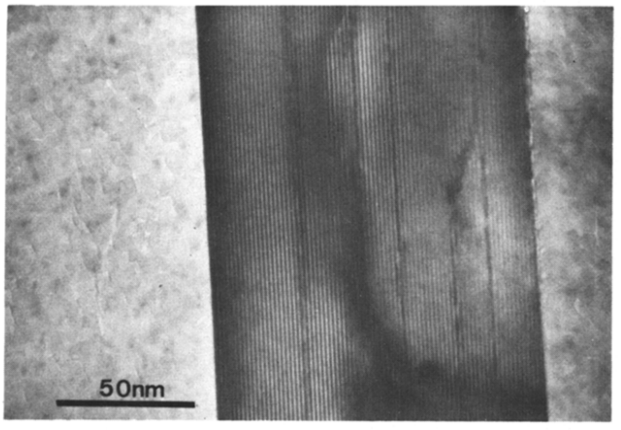

Fig. 5. High-resolution electron micrograph of a $Bi_4Ti_3O_{12}$ rod. The lattice fringes belong to (002) planes ($d_{002} = 1{\cdot}64$ nm).

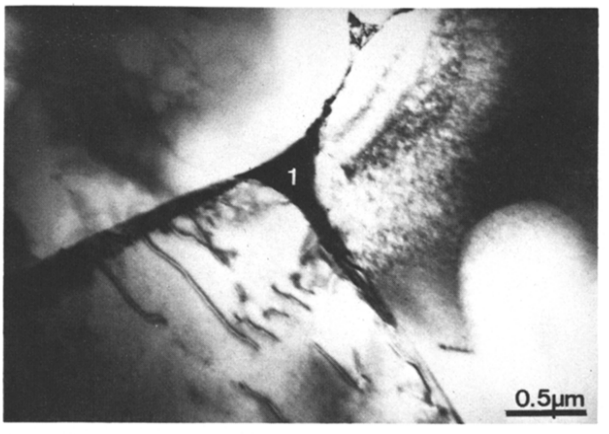

Fig. 7. Transmission electron micrograph. Bright field sample A quenched from 1100°C. ZnO grains with dislocations. Unidentified intergranular phase (1).

3.2.1.2 Quenched from 1100°C. Two phases were mainly observed: ZnO and an unidentified intergranular phase (Fig. 7). No $Bi_4Ti_3O_{12}$ was detected. The ZnO grains (grain size ranging from 4 to 80 μm) contain the usual lattice defects resulting from quenching. The amorphous or nanocrystalline state is also observed in some grains (Fig. 8). The unidentified phase was analysed and had the following mean atomic composition (cations only): Zn: 35–45 at.%, Bi: 35–45 at.%, Ti: 18–22 at.%. The crystal structure of this ternary oxide remains unknown. This compound was generally amorphous, giving only two broad diffraction rings, corresponding to $d_1 = 0{\cdot}300 \pm 0{\cdot}010$ nm and $d_2 = 0{\cdot}168 \pm 0{\cdot}005$ nm. Occasionally crystallized grains of the phase give spot diffraction patterns; the main interplanar distances measured on these are: $0{\cdot}380 \pm 0{\cdot}009$ nm, $0{\cdot}275 \pm 0{\cdot}008$ nm and $0{\cdot}225 \pm 0{\cdot}007$ nm.

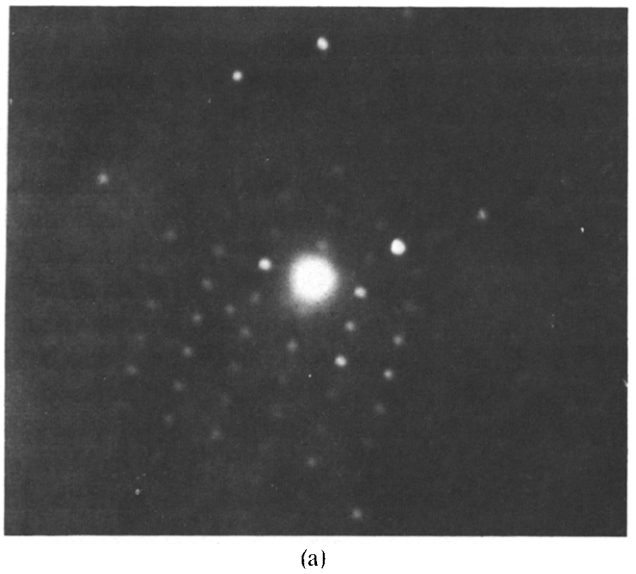

(a)

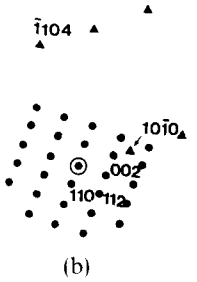

(b)

Fig. 6. (a) Transmission electron diffraction pattern of a γ-Bi_2O_3 grain. (b) Interpretation. (●) Reflections of γ-Bi_2O_3 oriented with [1$\bar{1}$0] parallel to the electron beam. (▲) Reflections of the ZnO matrix.

3.2.2 Series B samples

3.2.2.1 Quenched from 900°C. In this sample, two phases were observed: ZnO grains (grain size ranging from 0·1 to 1·5 μm) with dislocations and small rods (length = 0·5–1 μm) of $Bi_4Ti_3O_{12}$ (Fig. 9). No other intergranular phase was observed. All Bi and Ti atoms seem to be localized in the $Bi_4Ti_3O_{12}$.

3.2.2.2 Quenched from 1030°C. Besides the two phases already mentioned (ZnO and $Bi_4Ti_3O_{12}$), an unknown intergranular phase was observed (Fig. 10). ZnO appears both in the crystalline and the amorphous state. The grain size ranges from 0·5 to 5 μm. Numerous lattice defects were present. Some $Bi_4Ti_3O_{12}$ rods (0·1–0·2 μm in width, about 1 μm in length), located on ZnO grain boundaries were

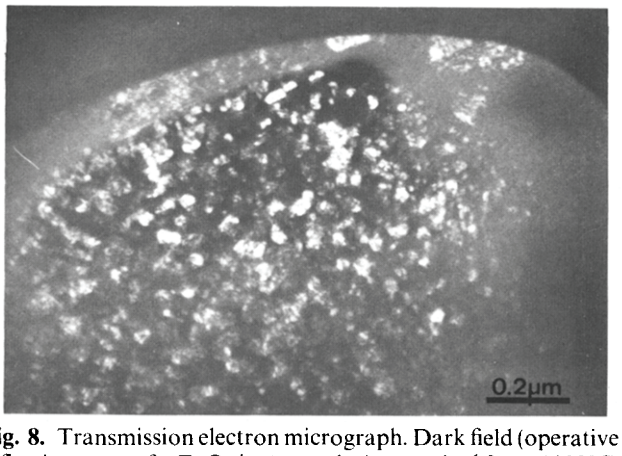

Fig. 8. Transmission electron micrograph. Dark field (operative reflection: part of a ZnO ring) sample A quenched from 1100°C. Nanocrystallized ZnO (grain size = 10–20 nm).

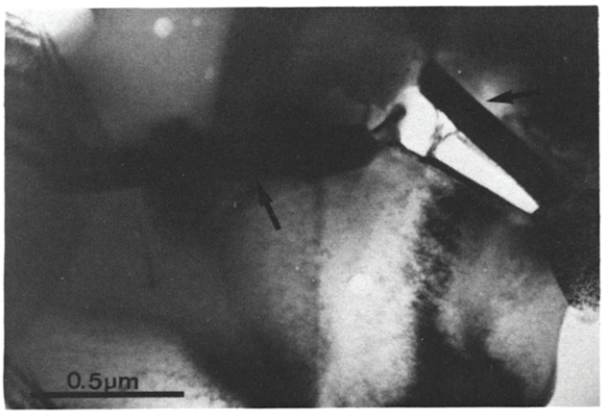

Fig. 9. Transmission electron micrograph. Bright field sample B quenched from 900°C. Grains of ZnO and rods (→) of $Bi_4Ti_3O_{12}$.

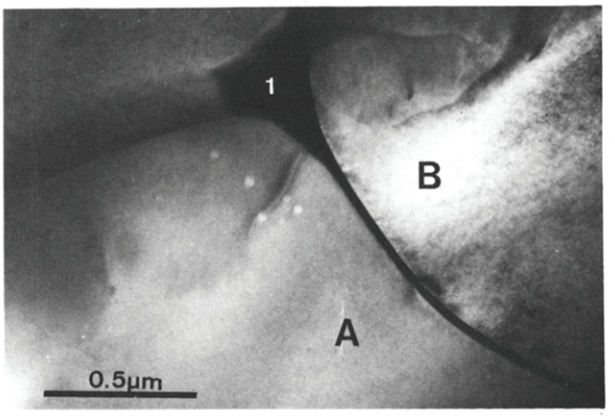

Fig. 11. Transmission electron micrograph. Bright field sample B quenched from 1100°C. Unidentified intergranular phase (1) forming a wetting layer on a ZnO grain boundary.

identified both by electron diffraction and microanalysis. The unidentified phase is always crystalline but the authors did not succeed in identifying its crystal structure. The main interplanar distances were: 0·402 ± 0·010 nm, 0·380 ± 0·010 nm, 0·315 ± 0·010 nm, 0·291 ± 0·008 nm, 0·268 ± 0·008 nm, 0·245 ± 0·007 nm, 0·201 ± 0·006 nm and 0·171 ± 0·005 nm. This oxide phase has a wide range of atomic composition: Bi: 45–55 at.%, Zn: 20–30 at.%, Ti: 20–25 at.%.

3.2.2.3 Quenched from 1100°C. Three phases were present: ZnO, the unidentified phase (Fig. 11) and the spinel cubic phase α-Zn_2TiO_4 (Fig. 12(a) and (b)). ZnO was always rich in lattice defects and presented some grains in the amorphous state. The grain size ranged from 2 to 20 μm. The unknown intergranular phase was crystalline and had a very wide atomic composition range (Bi: 35–50 at.%, Zn: 45–60 at.%, Ti: 2–5 at.%). It looks as though this phase has the same structure as in the preceding sample, since several of the interplanar distances were similar: 0·530 ± 0·015 nm, 0·395 ± 0·010 nm, 0·375 ± 0·010 nm, 0·318 ± 0·009 nm, 0·295 ± 0·008 nm, 0·280 ± 0·008 nm and 0·185 ± 0·006 nm. On multiple grain junctions, submicronic grains either monocrystalline (Fig. 12(a)) or nanocrystalline (Fig. 12(b)) were observed. The main interplanar distances given by the electron diffraction patterns on nanocrystalline grains are listed in Table 1, together with the theoretical lines of α-Zn_2TiO_4[14] and $Zn_2Ti_3O_8$,[15] and with the X-ray powder lines of α-Zn_2TiO_4 observed in samples B. It is clear that the $Zn_2Ti_3O_8$ phase is likely to be present in these grains, owing to

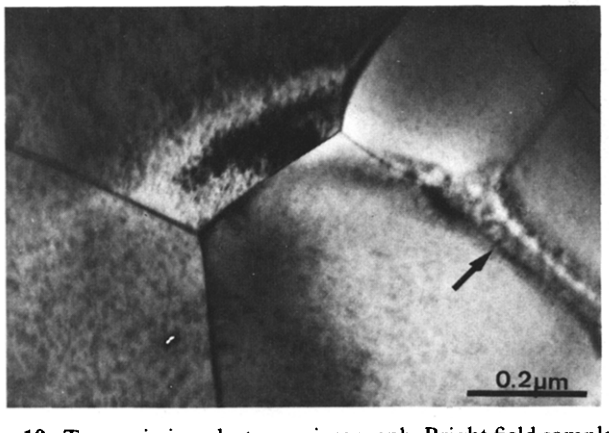

Fig. 10. Transmission electron micrograph. Bright field sample B quenched from 1030°C. Unidentified intergranular precipitate (→).

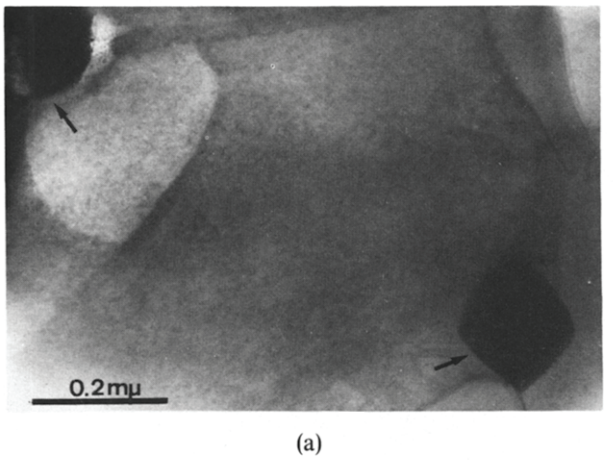

(a)

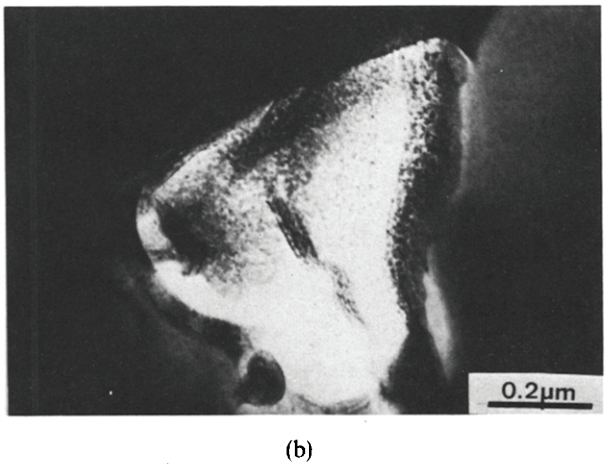

(b)

Fig. 12. Transmission electron micrograph. Bright field sample B quenched from 1100°C. (a) Monocrystalline grains (→) of α-Zn_2TiO_4; (b) nanocrystallized grains of α-Zn_2TiO_4 and $Zn_2Ti_3O_8$.

Table 1. Theoretical and observed interplanar distances of α-Zn_2TiO_4 (cubic spinel $a = 0{\cdot}8402$ nm[14]) and $Zn_2Ti_3O_8$ (cubic $a = 0{\cdot}8428$ nm[15])

α-Zn_2TiO_4		$Zn_2Ti_3O_8$		$d_{observed}$ nm	
$d_{theoretical}$ (nm)	*hkl*	$d_{theoretical}$ (nm)	*hkl*	*Electron diffraction*	*X-Ray diffraction*
—	—	0·3441	211	0·340	—
0·2991	220	0·2980	220	—	0·2996
0·2551	311	0·2541	311	0·254	0·2554
—	—	0·2253	321	0·223	—
0·1727	422	0·1721	422	0·172	—
0·1496	440	0·1490	440	0·149	0·1495
0·1430	531	0·1425	531	0·142	—
0·1131	642	0·1126	642	0·114	—

the experimental evidence of (211) and (321) lines. However, as these latter lines were not observed by X-ray powder diffractometry, it can be concluded that only a few crystallites of $Zn_2Ti_3O_8$ were present in these grains.

Finally, it is noteworthy that EDX microanalysis on ZnO grains, on both series A and B, did not reveal the existence of Bi or Ti atoms. Nevertheless, the detection threshold of these atoms (0·1 at.%) is relatively high. Thus from the quantitative measurements it is not possible to conclude that all the Bi or Ti atoms are fully localized in the minor phases, and are not present in the ZnO matrix or at the ZnO grain boundaries.

4 Discussion

4.1 Phase structures

From the structural point of view, TEM observations generally confirm the X-ray diffraction results (cf. Tables 2a and 2b).

Bismuth oxides were observed in the samples of series A: β-Bi_2O_3[12] (initial powder and after quenching at 750°C) and γ-Bi_2O_3[13] (after quenching at 750°C). These oxides, usually metastable at room temperature, were probably stabilized by a low content of Zn and/or Ti atoms, but the accuracy of the data does not allow the detection of the lattice constant changes reported in Ref. 16. At 750°C, the $\beta \rightarrow \gamma$ transition seems to be favoured. At higher temperatures, the bismuth oxide was no longer detected by X-ray diffraction in ceramics A. In fact, a very small proportion of this oxide is present in the sample and the Bi-rich melt is badly crystallized after quenching. However, some occasional grains of γ-Bi_2O_3 located on multiple grain junctions were observed by TEM at 900°C in ceramics A.

In series B, bismuth oxide was never identified whatever the quenching temperature, but an overall content of bismuth oxide lower than the detection threshold (0·1 mol% Bi_2O_3 for X-ray measurements) cannot be ruled out.

The binary oxide $Bi_4Ti_3O_{12}$ is present in all samples of both series A and B as early as 750°C but it only acquires a well-crystallized form (narrow X-ray lines) from 850–900°C. Notice that traces of this oxide were detected in powder where the overall Ti

Table 2a. Phases detected by X-ray and electron diffraction for series A (Ti = 0·6 at.%)

	X-Ray diffraction	*TEM*
Powder	β-Bi_2O_3	
750°C	β-Bi_2O_3 + γ-Bi_2O_3 + $Bi_4Ti_3O_{12}$	
850–900°C	$Bi_4Ti_3O_{12}$	$Bi_4Ti_3O_{12}$ + rare γ-Bi_2O_3
1000°C	$Bi_4Ti_3O_{12}$	
1100°C	Phase X	Phase X

Table 2b. Phases detected by X-ray and electron diffraction for series B (Ti = 1 at.%)

	X-Ray diffraction	*TEM*
Powder	$Bi_4Ti_3O_{12}$	
750°C	$Bi_4Ti_3O_{12}$ + α-Zn_2TiO_4 (traces)	
900°C	$Bi_4Ti_3O_{12}$ + α-Zn_2TiO_4 (traces)	$Bi_4Ti_3O_{12}$
1030°C	$Bi_4Ti_3O_{12}$ + α-Zn_2TiO_4	$Bi_4Ti_3O_{12}$ + phase X
1100°C	α-Zn_2TiO_4 + phase X	α-$Zn_2TiO_4 \pm Zn_2Ti_3O_8$ (traces) + phase X

Phase X: unidentified phase.

content is a maximum (series B: 1 at.% Ti). The amount of $Bi_4Ti_3O_{12}$ is maximum in the ranges 850–900°C and 1000–1030°C. Only small traces seem to remain at 1100°C for series A, whereas for series B no traces were identified at this temperature. This observation shows that, in both series, $Bi_4Ti_3O_{12}$ decomposes between 900°C and 1100°C. This decomposition probably occurs around 1030°C, as it is proposed by Makovec & Trontelj[5] who have detected an endothermic peak at this temperature by differential thermal analysis (DTA) experiments. In addition, the present results refute the interpretation of Kiseleva *et al.*:[6] they postulated the melting of $Bi_4Ti_3O_{12}$ in similar systems (also including cobalt, manganese and nickel oxides) around 1200°C.

These $Bi_4Ti_3O_{12}$ grains, having a plate-like shape, with the (001) plane parallel to the longitudinal axis, were only observed on the ZnO boundaries. Their size increases with the ZnO grain size but does not exceed $0{\cdot}3 \times 1\ \mu m^2$. That compound was never identified as an inclusion inside the grains, may be due to a lower overall Ti content (maximum 1 at.%) than in the Makovec & Trontelj samples[5] (minimum $Bi_4Ti_3O_{12}$ content 6%, probably in weight). On the other hand, it is well known that the preferential growth of $Bi_4Ti_3O_{12}$ crystallites is related to the high surface energy anisotropy.[17]

The Zn_2TiO_4 cubic spinel was only detected by X-ray diffraction in samples of series B with the richer overall Ti content (1 at.% Ti), first as traces in the range 750–900°C, then well crystallized between 1030°C and 1100°C. The maximum of α-Zn_2TiO_4 amount was observed at this later temperature. This spinel binary oxide was identified by TEM in samples quenched from 1100°C, as submicronic grains located on multiple grain junctions but never as inclusions inside the grains as reported in Refs 2 and 3; this fact could be due to the lower overall Ti content. Some nanocrystalline grains seem to have the $Zn_2Ti_3O_8$ structure, which has been observed in similar systems.[6]

A phase which the authors did not succeed in identifying was observed in samples quenched from the highest temperatures. This phase was located on ZnO grain boundaries and on multiple grain junctions, sometimes in the amorphous or nanocrystalline state (series A, samples quenched from 900–1100°C, or series B, samples quenched from 1030°C), and sometimes in the monocrystalline state (series B, samples quenched from 1030–1100°C). This phase probably originates from solidification during quenching of the liquid phase which has been recorded in sintering studies.[9] It can be inferred from its geometry that an unequal wetting of the ZnO grains by the liquid phase has occurred at the quenching temperatures. The interplanar distances obtained from X-ray or electron diffraction measurements, and the quantitative analysis performed on this phase are listed together in Table 3. Taking into account the accuracy of the measurements, for samples B, the X-ray and electron diffraction data are in good agreement. Moreover, some interplanar distances are found to be identical for different quenching temperature or in different series (A or B) samples. This suggests the existence of a single phase which would be stable over a wide range of composition. In fact, for samples B, the Ti content in this phase decreases between 1030°C (20–25 at.%) and 1100°C (2–5 at.%) which can be related to the increase of the α-Zn_2TiO_4 content in the same temperature range. Below 1100°C, in the liquid phase of the samples B, a crystallization of α-Zn_2TiO_4 and/or $Zn_2Ti_3O_8$ occurs; thus this liquid phase becomes poorer in Ti and seems to crystallize better during quenching (series B quenched from

Table 3. Interplanar distances of the unidentified intergranular phase (ternary oxide)

	A (1100°C)		*B (1030°C)*		*B (1100°C)*	
	X-Ray	*TEM*	*X-Ray*	*TEM*	*X-Ray*	*TEM*
d_{hkl}	—	—	—	—	—	0·530
	—	—	—	0·402	—	0·395
	—	0·380	—	0·380	—	0·375
	0·3155	—	—	0·315	0·3155	0·318
	0·2997	—	0·3001	0·291	0·2996	0·295
	0·2742[a]	0·275	—	—	0·2739[a]	0·280
	0·2718[a]	—	—	0·268	—	—
	—	—	—	0·245	—	—
	—	0·225	—	—	—	—
	—	—	—	0·201	—	—
	—	—	—	—	—	0·185
	—	—	—	0·171	—	—
at.%	Zn: 35–45 Bi: 35–45 Ti: 18–22		Zn: 20–30 Bi: 45–55 Ti: 20–25		Zn: 45–60 Bi: 35–50 Ti: 2–5	

[a] Additional X-ray data obtained by powder diffractometry with monochromatized CuK_α.

1100°C) than the Ti-richer phase (series A quenched from 1100°C): the Ti atoms seem to play the part of crystallization inhibitors.

4.2 Sintering processes

From these structural results, it is possible to consider shrinkage phenomena and grain growth as a function of overall Ti content. The dilatometric curves previously obtained for both series of samples[9] are reported in Fig. 13(a) and (b). The occurrence of the liquid phase in the samples will be discussed first, then the grain growth.

4.2.1 Liquid phase occurrence

In the samples B, only a Bi_2O_3 amount lower than 0·1 mol% was present, most of the Bi atoms being combined with Ti atoms as $Bi_4Ti_3O_{12}$ binary oxide. The Ti atom excess in the ceramic with respect to the stoichiometry of this oxide is explained by the presence of α-Zn_2TiO_4 traces in the initial powder and in the sample quenched from 750°C. Owing to either the lack or the very small amount of Bi_2O_3 present, only a very small quantity of liquid phase can appear between 700 and 950°C. In fact, during the sintering study of Bi-doped ZnO powders, it has been shown[9] that, with 0·2 at.% Bi, a liquid phase occurs only above 950°C. Ceramics B undergo a shrinkage that begins about 950°C and its rate is at a maximum at 1030°C (Fig. 13(b)). A quantity of the liquid phase, sufficient to allow a rearrangement to occur, therefore appeared in the sample in this temperature range. Most of the liquid phase probably originates from the reaction proposed by Makovec & Trontelj,[5] in agreement with the present microstructural observations:

$$6ZnO_{(solid)} + Bi_4Ti_3O_{12(solid)} \rightarrow 3Zn_2TiO_{4(solid)} + 2Bi_2O_{3(liquid)} \quad (1)$$

However, in the present experiments, liquid Bi_2O_3 was not observed, but rather a bismuth oxide-rich liquid phase, also containing Zn and Ti atoms (Table 3). This liquid oxide becomes poorer in Ti atoms between 1030 and 1100°C. This reaction therefore seems to occur in two stages:

$$ZnO + Bi_4Ti_3O_{12} \xrightarrow{900\ 1030\ C} \text{(Ti-rich Bi, Ti, Zn-melt oxide)} + xZn_2TiO_4 \quad (2a)$$

$$\text{(Ti-rich Bi, Ti, Zn-melt oxide)} \xrightarrow{1030\ 1100\ C} \text{(Ti-poor Bi, Ti, Zn-melt oxide)} + yZn_2TiO_4 \quad (2b)$$

Reaction (1) was detected by DTA experiments around 1030°C,[5] whereas in the present case shrinkage begins at 950°C. Two hypotheses could explain this result:

(i) Reaction (2a) begins about 950°C and continues with very slow kinetics until 1030°C, progressively releasing the liquid phase.

(ii) Reaction (2b) occurs around 1030°C and Bi_2O_3 traces (content <0·1 mol%) are responsible for the shrinkage beginning.

Only DTA experiments, performed on the present samples, would be conclusive.

The hypothesis of a shrinkage beginning due to bulk diffusion in the solid phase has been ruled out because of the rapid kinetics of the phenomenon. Moreover, these bulk diffusions generally begin at much lower temperatures about 700°C in undoped ZnO or Bi-doped ZnO powders.[9]

Samples A contained a small amount of Bi_2O_3 but sufficient to create a liquid phase activating the rearrangement after about 800°C (Fig. 13(a)). The $Bi_4Ti_3O_{12}$ decomposition then occurs between 950°C and 1100°C, releasing a supplementary amount of liquid phase. However, no binary Zn and Ti oxide was detected at 1000 or 1100°C. Up to 1100°C, the mechanism for this composition can only be described by reaction (3):

$$ZnO_{(solid)} + Bi_4Ti_3O_{12(solid)} + \text{(Bi-rich melt)} \xrightarrow{900-1100\ C} \text{(Ti-rich Bi, Ti, Zn-melt oxide)} \quad (3)$$

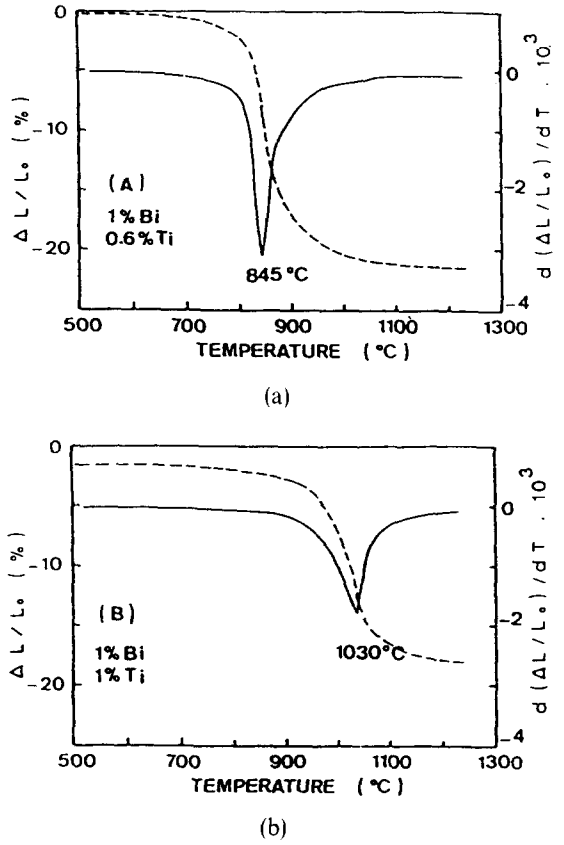

Fig. 13. Dilatometric curves:[9] dimension changes $\Delta L/L_0$ (- - - -) and the derived curve $d(\Delta L/L_0)/dT$ (——) as a function of temperature during sintering of samples. (a) Sample A, (b) sample B.

4.2.2 Grain growth

At 900°C, ceramics B were still very porous. Numerous pores were observed by scanning electron microscopy (SEM) and shrinkage was not achieved (Fig. 13(b)). From SEM images, it was noted that the grain size (0·1–1·5 μm) was higher than that of the primary particles of the initial powder (<0·1 μm). Grain growth has then occurred without shrinkage; the corresponding mechanism is probably surface diffusion in the solid phase. At 1100°C, shrinkage is very advanced and the grain size of the ceramics B ranges from 2 to 20 μm.

No systematic study of the ZnO grain boundary wetting by the liquid phase has been performed in the present experiments. However, it is well known that wetting varies with grain boundary surface energies, which are functions of the grain orientations.[18] On the other hand, wetting is marked when the liquid phase composition is close to that of the solid phase,[19] i.e. in the present case, when the Zn content increases in the liquid phase.[20] The authors have effectively found a significant amount of wetted grain boundary in the samples quenched from 1100°C (Figs 7 and 11), which corresponds to the highest Zn content in the liquid phase (Table 3), that is 35–45 at.% for series A and 45–60 at.% for series B.

In Fig. 11, the intergranular phase is clearly visible as the grain boundary plane is parallel to the electron beam direction. The width of this phase is regular and equal to 25 nm. The growth of the larger grain (A), revealing a concave surface, must be carried out to the detriment of the smaller grain (B) which presents a convex surface by a dissolution–precipitation mechanism.[21] A concentration gradient would therefore exist in the liquid phase, which could be determined by EDX nanoanalysis with a sufficiently narrow electron probe (1 nm). Quantitative analysis, performed with a larger probe (10–20 nm in diameter) on intergranular phases located on multiple grain junctions and having a greater size (0·5–1 μm) has not allowed evidence of a significant concentration gradient to be found.

For ceramics A, at 900°C, the grain size ranges from 0·2 to 2 μm and reaches 4–80 μm at 1100°C, i.e. the grain sizes are much greater than those of ceramics B (2–20 μm) at the same temperature. At 1100°C, the grains of ceramics B therefore show an important growth delay with respect to those of ceramics A. The more rapid growth in ceramics A could be explained by the releasing of a supplementary amount of liquid phase during the decomposition of $Bi_4Ti_3O_{12}$. The decomposition occurs in an already densified ceramic (Fig. 13(a)), i.e. presenting a very important grain boundary surface, and compensates for the liquid deficiency due to evaporation of the small initial amount of Bi-rich melt between 800°C and 1000°C. This more developed grain growth also increases the number of grain boundaries which are wetted by the liquid phase.

In contrast, in ceramics B, the liquid phase resulting from the $Bi_4Ti_3O_{12}$ decomposition is released in a very porous ceramic and widely contributes to its densification and simultaneously undergoes a significant evaporation so that growth mechanisms are delayed.

It has also been assumed that Ti atoms favour the reactivity of the liquid phase towards the ZnO grains.[3] Without being able to confirm the validity of this assumption, it can only be said that, with a higher overall Ti content (1 at.% Ti in series B), the liquid phase is poorer in Ti at 1100°C (2–5 at.%) than in series A (0·6 at.% Ti) where the liquid phase has a content of 18–22 at.%. However, at this temperature (1100°C), the Ti-poorest liquid phase is always richer in Zn (45–60 at.% Zn in samples B and 35–45 at.% Zn in samples A). Only a more detailed study, including a fine analysis of the intergranular phases, would allow a better understanding of this problem.

After a complete cycle of thermal treatment with a 6-h annealing at 1250°C, the grain size of ceramic A (mean size 100 μm) is nearly twice that of ceramics B.[9] It is then likely that the high Ti content in the liquid phase at 1100°C in ceramics A favours the dissolution–precipitation mechanism kinetics. These rapid kinetics are obtained with a reduced overall Ti content (0·6 at.% Ti), which avoids α-Zn_2TiO_4 crystallization and Ti impoverishment of the liquid phase. On the other hand, it is possible that the α-Zn_2TiO_4 spinel observed on multiple grain junctions is an inhibitor of grain growth.

5 Conclusion

Many minor phases have been identified in Bi–Ti-doped ZnO ceramics quenched during sintering between 750 and 1100°C: β- and γ-Bi_2O_3, plate-like grains of $Bi_4Ti_3O_{12}$, submicronic grains of α-Zn_2TiO_4 spinel and $Zn_2Ti_3O_8$. An unidentified phase, either amorphous or crystalline, originating from solidification of the melt phase, is stable over a wide range of composition. No minor phases were located within ZnO grains.

Contrary to published results relating to ceramics prepared by oxide mixture, the authors have found sintering processes are different for Bi–Ti-doped ZnO according to Ti content:

—With the greater Ti content (equal to Bi content), all Bi is initially combined with Ti in $Bi_4Ti_3O_{12}$ between 950 and 100°C, releasing a melt phase, thus allowing shrinkage only after 950°C; this shrinkage delay leads to a grain

growth delay. Moreover, Ti content in the melt phase decreases between 1000°C and 1100°C because of the α-Zn_2TiO_4 crystallization.

—With the lower Ti content, Bi_2O_3 quantity is sufficient to create a melt phase and thus to allow shrinkage as soon as 800°C is reached. The supplementary amount of liquid released by $Bi_4Ti_3O_{12}$ decomposition enhances the wetted grain boundary surface and thus grain growth. Because no α-Zn_2TiO_4 crystallization occurs, the melt phase remains Ti-rich and thus could also enhance grain growth.

Acknowledgement

The authors would like to thank L. Bernard of I.N.S.A., URA 74 for sample preparation for TEM.

References

1. Matsuoka, M., *Jpn J. Appl. Phys.*, **10** (1971) 736–46.
2. Trontelj, M., Kolar, D. & Krasevec, V., *J. Microsc. (Oxford)*, **124** (1981) 285–9.
3. Trontelj, M., Kolar, D. & Krasevec, V., In *Advances in Ceramics*, Vol. 7, ed. M. F. Yan & A. M. Heuer. American Ceramic Society, Columbus, OH, 1983, pp. 107–16.
4. Trontelj, M. Kolar, D. & Krasevec, V., *British Ceram. Process*, **36** (1985) 143–51.
5. Makovec, D. & Trontelj, M., In *Materials Science Monographs*, Vol. 66, ed. P. Vincenzini. Elsevier Science Publishers, Amsterdam, 1991, pp. 2137–45.
6. Kiseleva, L. A., Pavlotskii, Ya. V., Budim, N. I., Polyanskii, A. V. & Medvedev, F. K., *Izvestiya Akademii Nauk SSSR, Neorganicheskie Materialy*, **25** (1989) 2069–72.
7. Sung, G. V. & Kim, C. H., in *Advances in Ceramics*, Vol. 2, ed. M. F. Yan & A. M. Heuer. American Ceramic Society, Columbus, OH, 1987, pp. 841–7.
8. Rousset, A., Andrianjatovo, H. & Legros, R., Oxyde de zinc dopé. French Patent 900789, 1992.
9. Peigney, A., Andrianjatovo, H., Legros, R. & Rousset, A., *J. Mater. Sci.*, **27** (1992) 2397–405.
10. Mesnier, M. T. & Niepce, J. C., In *4ème Colloque International sur les Méthodes Analytiques par Rayonnements X*, C.G.R., Strasbourg, 9–13 Mai 1977.
11. Correia Neves, J., Lopes, J. E., Sahama, T. G., Lehtinen, M. & Knorring, O. V., *Rev. Cien. Geol. Ser. A*, **7** (1974) 1–37.
12. Medernach, J. W. & Snyder, R. L., *J. Am. Ceram. Soc.*, **61** (1978) 494–7.
13. Cummins, S. E. & Cross, L. E., *J. Appl. Phys.*, **39** (1968) 2268–74.
14. N.B.S. Monograph, **25** (1974) 37.
15. Reddy, V., *Mater. Chem. Phys.*, **10** (1984) 365.
16. Levin, E. M. & Roth, R. S., *J. Res. Nat. Bureau Standards, A, Phys. Chem.*, **68A** (1964) 197–206.
17. Takenaka, T. & Saraka, K., *Jpn J. Appl. Phys.*, **19** (1980) 31–9.
18. Clarke, D. R., *J. Appl. Phys.*, **49** (1978) 2407–11.
19. Smith, C. S., *Trans. Am. Inst. Min. Metall. Engng.*, **175** (1948) 15–5 .
20. Gambino, J. P., Kingery, W. D., Pike, G. E., Levison, L. M. & Philipp, H. R., *J. Am. Ceram. Soc.*, **72** (1989) 642–5.
21. German, R. M., *Liquid Phase Sintering*. Plenum Press, New York, 1985.